

Numerical Analysis of 100mm Naval Gun Barrel Composite Cooling Based on Multiphase Flow

Xinyun Liu, Dalin Wu, Jian Hou

Abstract—Active cooling technology is widely used in naval gun. The composite cooling system with external circulating water cooling technology and internal spray cooling technology is adopted for 100mm medium caliber naval gun. In order to optimize the cooling efficiency of barrel and improve the combat effectiveness and safety performance of naval gun, it is of great significance to study the internal fluid field and barrel temperature field under the condition of composite cooling. Regarding 100mm naval gun as the object of the research, this paper proposed to use numerical analysis method combining classical interior ballistics with computational fluid dynamics to establish the transient CFD three-dimensional model based on multiphase flow. Physical quantities such as temperature, velocity, species distribution, and interphase mass transfer in the calculation domain were calculated through simulation, and the temperature changes of the barrel with and without the cooling system were compared and analyzed. Finally, the laws of the gun barrel were obtained, which provided references for further study.

Index Terms—Naval gun barrel, Composite cooling, Multiphase flow, Numerical analysis, Coupling heat transfer, Temperature field

I. INTRODUCTION

The composite cooling process of the gun barrel is very complicated, and the numerical simulation analysis involving internal spray cooling and external circulating water cooling is a difficult point. Modern naval gun constantly increases the firing rate, which can lead to many reliability problems caused by the rapid rise of barrel temperature, such as the shortening of barrel life, the reduction of firing accuracy, and even spontaneous combustion and explosion. Natural cooling has been far to meet the performance requirements of modern naval gun, therefore it is necessary to adopt active cooling methods to cool down the barrel. Common active cooling includes external cooling, mid-wall cooling and internal cooling [1]. The combination of two or more cooling methods is called composite cooling, which combines the advantages of different cooling methods and can achieve higher

comprehensive cooling efficiency. This paper focuses on the composite cooling system of 100mm naval gun, and studies how to obtain important parameters and laws by numerical simulation analysis [2]-[3].

Many scholars studied the heating and active cooling of barrel. However, most of them only studied barrel heating, external cooling or mid-wall cooling. L.M. Chen[4] used the one-dimensional interior ballistic model and MacCormack finite difference method to solve the heating process of composite barrel. Ercan Degirmenci[5] established a heat transfer finite element model of the NATO standard small caliber barrel of 7.62 mm in diameter and analyzed the effects of various grain sizes and initial temperatures. W. Wang[6] established a finite element model of barrel heat transfer and obtained the relationship between barrel temperature rise and many factors, such as firing rate, firing mode, environmental temperature. Y.H. Wu[7] established an external circulating water cooling model for the rapid-fire gun, and the outer wall adopts the coupling heat transfer. L.J. Zhang[8] established an external circulating water cooling model for 130mm large caliber naval gun, and the outer wall adopts the third boundary condition of convective heat transfer. B. Wu[9]-[10] established an unsteady heat transfer finite element model for 155mm large caliber gun with mid-wall cooling system, and analyzed the relationship between cooling effect and wall thickness, heat transfer coefficient respectively. J.G. Zhao[11] established a finite element model of external noncirculating water vaporization cooling for rapid-fire gun, and analyzed the feasibility of the cooling method. In the above studies, the average temperature curve of propellant gas is obtained through the interior ballistic equation and the empirical formula of after-effect period, and the convective heat transfer coefficient of the whole time history is calculated. They determine the boundary conditions of the inner wall, simplifying and avoiding the complicated internal fluid domain with high temperature and high pressure. X.H. Wang[12] established a CFD model for 155mm naval gun with external water cooling, internal air cooling and mid-wall water cooling. The boundary conditions of internal high-temperature propellant gas fluid domain were considered as breech pressure inlet and muzzle pressure outlet. T.T. Zhao[13] established a multiphysics coupling model of barrel, and the boundary conditions of internal high-temperature propellant gas fluid domain were considered as breech velocity inlet and muzzle pressure outlet.

Although the internal fluid domain was considered in the above studies, they simply considered the internal fluid domain as the channel of the breech inlet-muzzle outlet mode, which cannot accurately obtain the distribution and change of

Manuscript received August 13, 2019; revised March 31, 2020. This work was supported in part by Foundation of PLA Naval Equipment Research Institute.

Xinyun Liu is with Shijiazhuang Campus, Army Engineering University 050003 China (corresponding author to provide e-mail: 251815902@qq.com).

Dalin Wu is with Shijiazhuang Campus, Army Engineering University 050003 China (e-mail: dalinwu@163.com).

Jian Hou is with Naval University of Engineering 430033 China. (e-mail: 501-hj@163.com).

various parameters. At present, there is no more accurate numerical analysis method considering the internal fluid domain of the barrel, nor the calculation method considering both internal spray cooling and external circulating water cooling.

In this paper, a CFD numerical analysis method for composite cooling systems was proposed, which can accurately calculate and predict the results of typical parameters. The method analyzed the internal fluid domain and the external solid domain simultaneously based on multiphase flow, considering factors such as liquid evaporation, phase interaction, species diffusion, etc. According to classical interior ballistics and computational fluid dynamics, the whole firing process was divided into two periods for calculation. The changes of the boundary conditions of the internal fluid domain during the whole firing action were considered in detail, including the boundary of the projectile movement, the boundary of the cartridge movement, and the boundary of each spray inlet.

II. MATHEMATICAL MODEL

A. Governing equation of multiphase fluid

Multiphase flow follows three basic physical laws: the law of mass conservation, the law of momentum conservation and the law of energy conservation. The following three governing equations are called continuity equation, Navier-Stokes equation and energy equation (1) [14]-[16].

$$\left\{ \begin{array}{l} \frac{\partial \rho_m}{\partial t} + \nabla \cdot (\rho_m V_m) = 0 \\ \frac{\partial V_m}{\partial t} + \nabla \cdot (V_m V_m) = f_b - \frac{1}{\rho_m} \nabla p + \frac{\mu_m}{\rho_m} \nabla^2 V_m + \frac{1}{3} \frac{\mu_m}{\rho_m} \nabla (\nabla \cdot V_m) \\ \frac{\partial (\rho_m h)}{\partial t} + \nabla \cdot (\rho_m h V_m) = -p \nabla \cdot V_m + \nabla \cdot (\lambda_m \nabla T) + \Phi + S_h \end{array} \right. \quad (1)$$

Where, ρ_m is the multiphase fluid density, V_m is the multiphase fluid velocity vector, f_b is the body force, p is the differential pressure, μ_m is the multiphase fluid dynamic viscosity, h is the specific enthalpy, λ_m is the multiphase fluid heat conductivity coefficient, Φ is the viscous dissipation term, S_h is the source terms [17]-[18].

B. The boundary conditions of convective heat transfer

During the interior ballistic period, the third boundary of convective heat transfer (2) that requires the heat transfer coefficient and fluid temperature at any time was applied to the inner and outer walls [19].

$$\left\{ \begin{array}{l} h_g (T_g - T) \Big|_{r=R_g} = -\lambda \frac{\partial T}{\partial r} \Big|_{r=R_g} \\ h_l (T - T_l) \Big|_{r=R_l} = -\lambda \frac{\partial T}{\partial r} \Big|_{r=R_l} \end{array} \right. \quad (2)$$

Where, h_g is the heat transfer coefficient of propellant gas and inner wall of barrel, h_l is the heat transfer coefficient of outer wall of barrel and external circulating water, external

air respectively, T_g and T_l are the temperature in the internal fluid domain and the external fluid domain respectively, R_g and R_l are the radius of inner wall and outer wall respectively [20].

During the non-interior ballistic period, the fourth boundary condition (3), namely coupled heat transfer, was applied to the inner wall. During this time, the temperature and heat flux at the fluid-solid interface are no longer known conditions and coupled in the calculation process. At the fluid-solid interface, the temperature and heat flux satisfy the continuity.

$$\left\{ \begin{array}{l} T_w \Big|_l = T_w \Big|_s \\ q_w \Big|_l = q_w \Big|_s \end{array} \right. \quad (3)$$

Where, W represents the fluid-solid interface, l and s represent the fluid domain and the solid domain respectively.

C. Heat transfer coefficient

The convective heat transfer boundary conditions of the outer wall surface are classified into two types: the outer wall in contact with the outside air and the outer wall in contact with the circulating cooling water. The outer wall in contact with the outside air is the natural convection heat transfer boundary. Firstly, the Grashof number is solved according to the Grashof criterion (4). Then the natural convection heat transfer Nusselt criterion (4) relation of the horizontal cylinder is determined according to the range of $GrPr$ [21].

$$\left\{ \begin{array}{l} Gr = \frac{g(T_w - T_\infty) D^3}{\nu^2 (273.15 + t_f)} \\ Nu = \left\{ 0.6 + \frac{0.387 (GrPr)^{1/6}}{[1 + (0.559 / Pr)^{9/16}]^{8/27}} \right\}^2 \end{array} \right. \quad (4)$$

Where, T_w is the wall qualitative temperature, T_∞ is the fluid qualitative temperature and T_f is the average qualitative temperature, D is the outer wall diameter of barrel, ν is the fluid kinematic viscosity.

The outer wall in contact with the circulating cooling water is the forced convection heat exchange boundary, which can be approximated as the forced convection heat transfer Nusselt criterion (5) of the longitudinal flow plate.

$$\left\{ \begin{array}{l} Re = \frac{\rho_l u_l l}{\mu} \\ Nu = 0.037 Re^{4/5} Pr^{1/3} \end{array} \right. \quad (5)$$

Where, ρ_l is the density of cooling water, u_l is the mean flow velocity of cooling water, l is the length of the outer wall in contact with the cooling water.

During the interior ballistic period, the inner wall in contact with the propellant gas is the forced convection heat transfer boundary, which can be approximated as the Nusselt criterion of convection heat transfer in the circular tube (6). According to Lagrange hypothesis, that is, the gas density is uniformly distributed and the velocity is linearly distributed

in the post-projectile space, it can be known that the gas density (7), temperature, dynamic viscosity and thermal conductivity in the post-projectile space are all functions of the time during the interior ballistic period, and the velocity of gas is a function of time and axial coordinates [22].

$$Nu(t, x) = 0.023 Re(t, x)^{0.8} Pr^{0.4} \quad (6)$$

$$\rho_g(t) = \frac{m_0 + m_q(t)}{W(t)} = \frac{\rho_0 \left(W_0 - W_1 - \frac{\omega}{\delta} \right) + \omega \psi(t)}{W_0 + Sx(t) - W_1 - \left[\frac{\omega}{\delta} (1 - \psi(t)) \right] - \alpha \omega \psi(t)} \quad (7)$$

Where, m_0 is the mass of the air in chamber before firing, m_q is the mass of the gas produced by propellant combustion. W is the volume of post-projectile space, W_0 is the volume of chamber, W_1 is the volume of metal cartridge case, ω is the charge, δ is the propellant density, ψ is the fraction of propellant burnt, S is the cross-sectional area of gun bore, x is the projectile motion displacement, α is the covolume, ρ_0 is the air density, ρ_g is the propellant gas density, u_g is the propellant gas velocity, d is the inner wall diameter.

The convective heat transfer coefficients of each wall are calculated from Nusselt number (8).

$$\begin{cases} h_{out} = \frac{Nu\lambda}{l} \\ h_{in}(t, x) = \frac{Nu\lambda(t)}{d} K_c \end{cases} \quad (8)$$

Where, h_{out} and h_{in} are the heat transfer coefficients of outer wall and inner wall respectively, K_c is the correction coefficient of thermal radiation.

D. Gas state equation

The equation of state expresses the mathematical relationship among the thermodynamic state functions. The most commonly used equation of state is the ideal gas state equation which is suitable for the environments of low pressure and high temperature. However, when the internal fluid domain is in a high pressure and high temperature environment, the ideal gas state equation becomes inaccurate. This model uses the Redlich-Kwong real gas state equation (9) [23].

$$P = \frac{RT}{V-b} - \frac{\alpha_0}{V(V+b)} \left(\frac{T_c}{T} \right)^{0.5} \quad (9)$$

Where, P is the absolute pressure, R is the universal gas constant, V is the molar volume, T is the temperature, T_c is the critical temperature, both α_0 and b are the constants related to critical temperature and pressure.

E. Species transport equation

The gas phase in the internal fluid domain contains three species: propellant gas, nitrogen and vapor. The flow and diffusion of the species are described by the turbulent species transport equation (10). The diffusion flux is mainly related to the concentration distribution and temperature distribution of the species. In this model, the internal fluid domain was activated from the end of the interior ballistic period and the chemical reaction between species was not considered in the

non-interior ballistic period.

$$\begin{cases} \frac{\partial}{\partial t} (\rho Y_i) + \nabla \cdot (\rho \bar{V} Y_i) = -\nabla \cdot \bar{J}_i + S_i \\ \bar{J}_i = - \left(\rho D_{i,m} + \frac{\mu_t}{Sc_t} \right) \nabla Y_i - D_{T,i} \frac{\nabla T}{T} \end{cases} \quad (10)$$

Where, Y_i is the mass fraction of i specie, \bar{J}_i is the diffusion flux of i specie, S_i is the rate of mass transfer from liquid phase, $D_{i,m}$ is the mass diffusion coefficient of the i specie in the m phase, $D_{T,i}$ is the thermal diffusion coefficient of the i specie, μ_t is the turbulent viscosity, Sc_t is the turbulence Schmidt number.

F. Evaporation-condensation model

The water vaporization was calculated by using the Lee evaporation-condensation mass transfer model [24]. When the water temperature is higher than the specified critical temperature, the liquid phase starts to convert into the gas phase, and when the vapor temperature is lower than the critical temperature, the gas phase starts to transform into the liquid phase. The vaporization mass transfer equation (11) and the conversion rate control equation (12) are as follows.

$$\frac{\partial}{\partial t} (\alpha_v \rho_v) + \nabla \cdot (\alpha_v \rho_v V_v) = \dot{m}_{lv} - \dot{m}_{vl} \quad (11)$$

$$\begin{cases} \dot{m}_{lv} = k_{lv} \cdot \alpha_l \rho_l \frac{T_l - T_{sat}}{T_{sat}} \\ \dot{m}_{vl} = k_{vl} \cdot \alpha_v \rho_v \frac{T_{sat} - T_v}{T_{sat}} \end{cases} \quad (12)$$

Where, v and l represent the gas phase and the liquid phase respectively, α is the volume fraction of a phase, V is the velocity vector of a phase, \dot{m}_{lv} and \dot{m}_{vl} are the mass transfer rates of evaporation and condensation respectively, T_{sat} is the specified critical temperature, k_{lv} and k_{vl} are the constants controlling relaxation time.

III. CFD MODELING

This research established the barrel heating and composite cooling model based on CFD software Fluent [25]. The turbulence model used SST two-equation model. The environment temperature of air and water was considered to be constant 20°C. The density of compressible mixed gas was described by real-gas-redlich-kwong state equation. Mixture model was applied to multiphase flow. The phase interaction included drag, slip velocity, surface tension and mass transfer. Due to the multiphase flow and species transport, the gravity effects should be considered.

A. Structure

Before calculating, it is important to understand the structure and working process of the model. Figure 1 is the schematic diagram of naval gun composite cooling system. The total length of the model is 5.5m. The external cooling water jacket covers the outer surface of the barrel, covering from the nitrogen inlet position to the position approaching the muzzle. The cooling water circulates in the water jacket, pipes and a certain volume of water storage tank. The water

inlet is behind, and the water outlet is in front. The eight high-pressure nitrogen inlets are axisymmetrically distributed, and the angle between the direction of inlets and the central axis is 45 degrees. The eight high-pressure water inlets are located underside of the barrel. In the front view, the inlet direction is at an angle of 45 degrees to the central axis. In the left view, the inlet direction is symmetrical, but the angles are different. The external circulating water cooling system works continuously during firing, and the internal spray cooling system only works briefly during the firing interval. When the propellant burns, the pressure expands the cartridge case that seals the nozzle. At this time, hydraulic valve of the nozzle is closed to prevent the high temperature and high pressure gas from flowing backward.

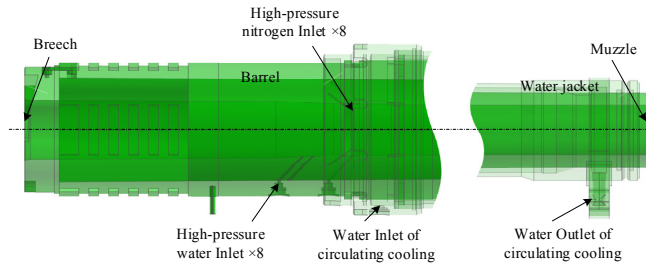


Fig. 1. Schematic diagram of naval gun composite cooling system

B. Meshing

Before meshing, the barrel CAD model was appropriately geometric processed to simplify the geometry model under the premise of ensuring the accuracy of the model. The barrel is the autofrettaged composite barrel and the interface between sleeve and barrel was not considered. In order to reduce the calculation amount, according to the symmetry of the barrel, only half of the model needs to be calculated. Ignoring the influence of rifling, the inner wall was regarded as smooth surface. According to the fluid domain characteristics near the nozzle, a merge mesh including the hexahedral structured mesh and the polyhedral unstructured mesh was applied, and the boundary layer mesh and the mesh near the nozzle were encrypted. As shown in Figure 2, the merge mesh interface and the fluid-solid interface transmitted data through Mesh Interface. The total number of grid cells is about 3.3 million.

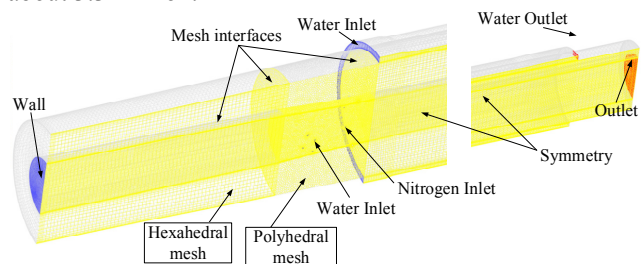


Fig. 2. Schematic diagram of the merge mesh

C. Boundary Conditions

The working time of spray cooling systems, the extraction time of cartridge case and the total time of firing cycle were obtained by analyzing the dynamic model of naval gun, and then boundary conditions of the model are determined. A firing cycle was divided into four periods:

(1) The interior ballistic period (0-0.0105s): The internal fluid domain was deactivated. The outer wall surface set

different boundary conditions according to two types of convective heat transfer. Free stream temperature of inner wall was controlled by Profile file. According to equations (6) and (7), the convective heat transfer coefficient of the inner wall is a function of time and displacement. This function was described in C language and controlled by UDF macro files.

(2) The period between the end of the interior ballistic period and the beginning of the internal spray (0.0105-0.0705s): The internal fluid domain was activated. During this period, the cartridge case extraction movement has not started. The breech, the water inlet and the nitrogen inlet were set as wall. The fluid-solid interface was set as couple heat transfer interface. According to Lagrange hypothesis, the internal fluid domain was initialized. The temperature was the average temperature at the end of the interior ballistic period. The velocity $v(x)$ and pressure $p(x)$ are determined by function (13). Where, L is the length of barrel, ω is the charge, m is the mass of the projectile, φ is the resistance coefficient, v_d is the projectile velocity at the end of the interior ballistic period, p_d is the projectile base pressure at the end of the interior ballistic period. The velocity and pressure distribution after initialization is shown in Figure 3.

$$\begin{cases} v(x) = v_d \frac{x}{L} \\ p(x) = p_d \left[1 + \frac{\omega}{2\varphi m} \left(1 - \frac{x}{L} \right)^2 \right] \end{cases} \quad (13)$$

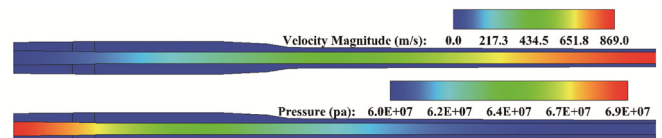


Fig. 3. Velocity and pressure of the fluid domain after initialization

(3) The internal cooling period (0.0705-0.3555s): During this period, the cartridge case was extracted, the water and nitrogen nozzle were exposed, and the water and nitrogen valve were opened. Therefore, the boundary conditions of water inlet and nitrogen inlet were changed from wall to mass flow inlet, and the boundary condition of breech was changed from wall to pressure outlet.

(4) The period between the end of internal spray and the end of firing cycle (0.3555-0.6855s): During this period, the boundary conditions of water inlet and nitrogen inlet changed from inlet to wall.

IV. NUMERICAL ANALYSIS AND DISCUSSION

Before the transient calculation, the steady calculation of the external cooling water flow is required to obtain the average flow velocity, that is, the heat transfer coefficient formula (5). The firing cycle time of the naval gun is 0.6855s, and the rate of firing is about 88 r/min. In order to further study the temperature changes of the barrel, it is necessary to analyze the model under continuous firing conditions. The analysis result of the last numerical calculation was used as the initial condition of the next calculation, and the continuous firing condition was simulated by continuous

calculation.

A. Species distribution

The fluid domain contains a mixture of water, vapor, nitrogen, and propellant gas, which mixes, phase changes and diffuses, affecting the pressure, velocity and temperature in the chamber. Therefore, it is necessary to analyze and discuss the changes of species distribution of the fluid domain. Due to the small difference in species distribution of each firing under continuous firing conditions, it is only necessary to select the first firing process for discussion.

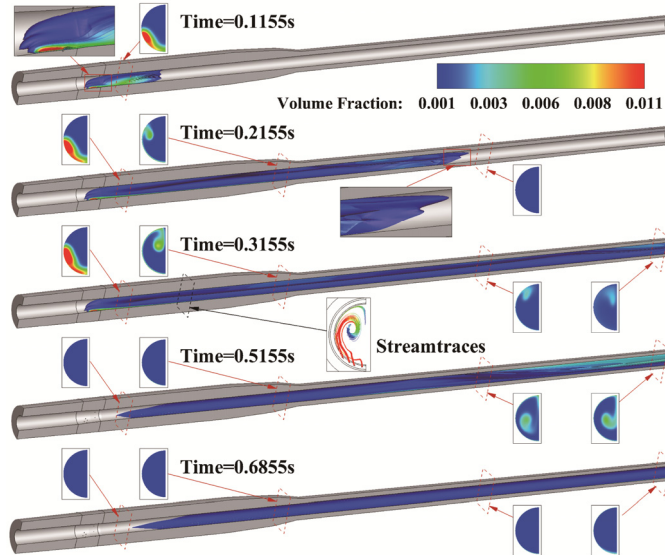


Fig. 4. Volume fraction of liquid water

Figure 4 shows the changes of volume fraction of the liquid phase in the fluid domain and cross section. The high-pressure water sprays from the nozzle at 0.0705s. Under the influence of internal high pressure, high temperature, high-speed propellant gas, high-pressure nitrogen, gravity and other factors, the water distribution in the above figure is formed. After the water enters, part of the water is vaporized into vapor due to high temperature, and the other part of the water moves rapidly toward the muzzle. The front end of the water movement is "convex". The cross sectional contours and streamlines show a "double spiral" motion of the water from bottom to top and from back to front. When the water enters for 285ms, the water spray valve is closed, and part of the water flows out of the muzzle. The water in the chamber gradually decreased.

Figure 5 shows the concentration changes of vapor in the fluid domain and cross section after water vaporization. Compared with the distribution of the water in Fig.4, the vapor in Fig.5 is concentrated in the front of water movement. This phenomenon is because that the temperature in the front of the water is the highest at the beginning, but as the movement and vaporization of the water, the gas temperature in the rear of the water rapidly drops below the critical vaporization temperature, and the vaporization rate decreases gradually. Therefore, the distribution of vapor appears to be "columnar" moving forward until it flows out of the muzzle.

Figure 6 shows the concentration changes of nitrogen in the fluid domain and cross section. The angle between the high-pressure nitrogen inlet and the axis is 45 degrees. Nitrogen enters from eight axisymmetric inlets, then mixes

evenly and move forward. The front end of the nitrogen movement is "concave". When the nitrogen gas enters for 285ms, the nitrogen valve is closed, and the remaining nitrogen gradually flows out of the muzzle, and the air enters from the breech. The concentration of nitrogen in the chamber decreases gradually.

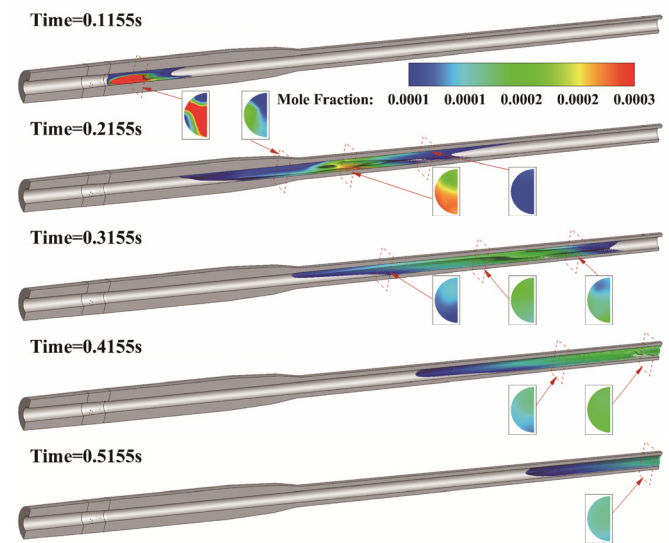


Fig. 5. Mole fraction of vapor

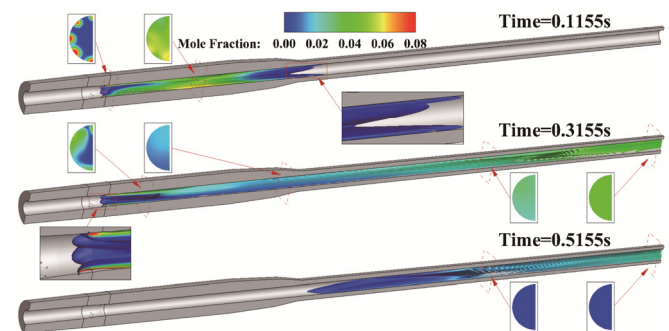


Fig. 6. Mole fraction of nitrogen

B. Velocity

The velocity calculation of the internal fluid domain begins at the end of the interior ballistic period. The velocity of the fluid in the chamber is initialized based on the calculation results of the interior ballistic and the Lagrange hypothesis of post-ballistic space.

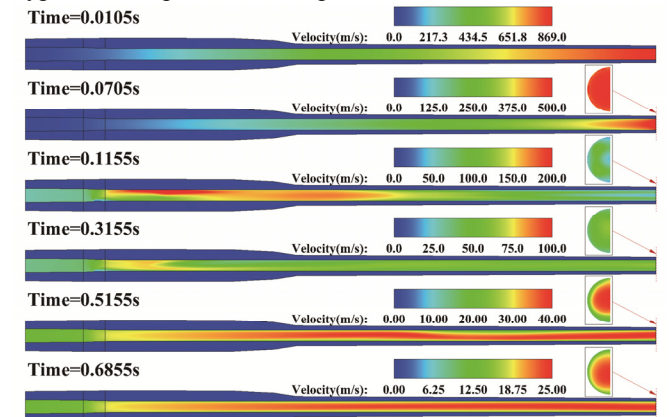


Fig. 7. Velocity distribution on the plane of symmetry

Figure 7 shows the velocity changes of the symmetry plane during the non-interior ballistic period. Before the internal

spray cooling system works, as the high pressure propellant gas flows out of the muzzle, the velocity of the internal fluid domain decreases gradually and presents a gradual distribution along the axis. When the spray starts, the boundary of breech opens, and the external air enters the fluid domain from the breech. The velocity near the nitrogen inlet is the highest, and the muzzle velocity becomes irregular from uniform distribution. When the spray stops, the velocity of the fluid domain decreases rapidly, and the velocity distribution in the muzzle becomes big on the center and small at the edge.

The velocity distribution in the fluid domain of the barrel is complex. From the end of the interior ballistic period to the start of the internal spray system, the overall velocity of the fluid domain is gradually decreasing and approximately maintains a gradual distribution from 0 m/s to maximum velocity; After the internal spray system starts working, the velocity distribution becomes chaotic, and the maximum velocity region in the fluid domain changes from the muzzle position to the nozzle position; As the internal spray system stops working, the velocity distribution in the fluid domain will gradually become regular.

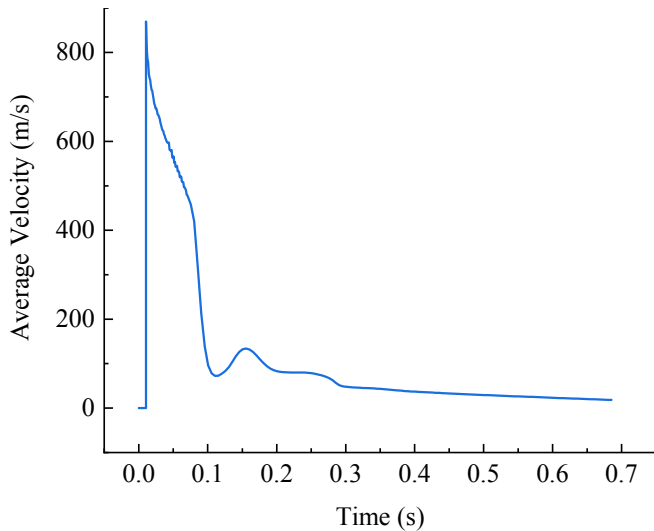


Fig. 8. Average velocity curve of muzzle

Figure 8 shows the average velocity monitoring curve of the muzzle fluid. At 0.0105s, the average fluid velocity of muzzle is the largest, reaching 870m/s, which is equal to the velocity of the projectile at this time. As the high pressure gas flows out, the muzzle velocity decreases rapidly. At 0.0705s, the spray cooling system starts to work. At this time, the boundary of breech is opened and the muzzle velocity decreases faster. Due to the entry of high-pressure water, high-pressure nitrogen and water vaporization expansion, the muzzle velocity reaches a minimum at about 0.11s and then begins to rise briefly. Subsequently, due to the rapid decrease of the temperature and vaporization, the muzzle velocity starts to decrease again after reaching a maximum, and stabilized at about 80 m/s. Finally, as the water and nitrogen valve is closed, the muzzle velocity begins to decrease gradually.

The average velocity of the muzzle reaches the maximum when the projectile leaves the muzzle, and then decreases rapidly. However, due to the presence of the internal spray

system, the average velocity of the mouth does not decrease all the time, but there is a stage of increase and then decrease. This is a typical feature with an internal cooling system.

C. Temperature

(1) Fluid domain temperature

The temperature calculation of the internal fluid domain also begins at the end of the interior ballistic period. The initial detonation temperature is 2380K, and the propellant gas temperature at the end of the interior ballistic drops to 1630K, which was used for temperature initialization. The changes of temperature are related to fluid flow, heat conduction, convective heat transfer and latent heat of phase change.

The internal cooling directly reduces the temperature in the internal calculation domain of the barrel (Fig.9). Before the water and nitrogen valve is opened, part of high temperature and high pressure gas in the chamber flows out from the muzzle, and the gas temperature decreases gradually. When the water valve, nitrogen valve and breech are opened, the nitrogen, water and external air enter the calculation domain and push the high temperature gas to the muzzle. The temperature of the internal fluid domain decreases rapidly from back to front. Most of the high temperature gas is pushed out of the muzzle at around 0.3s. Six coordinate positions were selected as monitoring points on the central axis of the internal fluid domain, and temperature changes of each point were recorded separately (Fig.10). The curve shows that the closer to the front of the barrel, the slower the temperature drop, which is consistent with the temperature distribution shown in Figure 8.

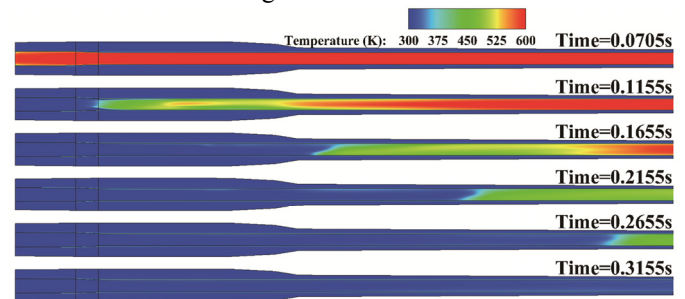


Fig. 9. Temperature distribution on the plane of symmetry

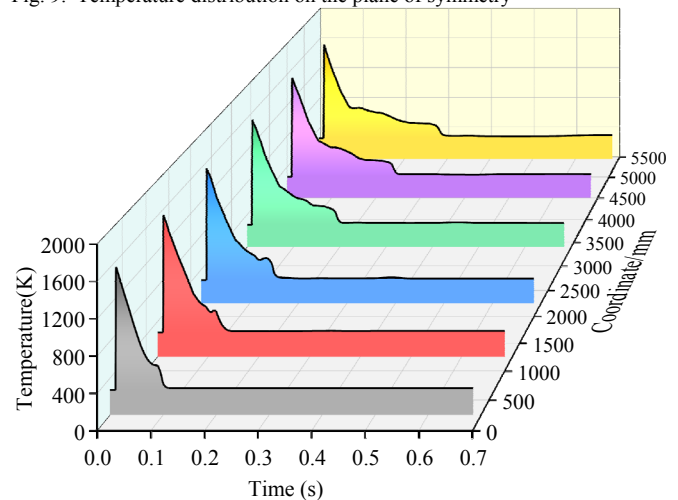


Fig. 10. Temperature curve of monitoring point in fluid domain

(2) Fluid-solid interface temperature

Figure 11 shows the temperature distribution changes of

fluid-solid interface during interior ballistic and non-interior ballistic periods. During the interior ballistic period, as the projectile moves, the inner wall behind the projectile begins to absorb heat. The temperature distribution from the breech to the bottom of the projectile is higher in the middle and lower on both sides. Moreover, the temperature of the inner wall increases first and then decreases, and the maximum temperature reaches 1097.6 K. During the non-interior ballistic period, the fluid-solid coupled heat transfer boundary was set. The temperature curve of the monitoring points on the fluid-solid interface (Fig.12) shows that the maximum temperature near the front of chamber throat (1.25m) is the highest, and as the X coordinates of the interface increases, the time to reach the maximum temperature becomes later and later. The interface at the back of barrel (coordinate less than 3.5m) reaches the maximum temperature in the interior ballistic period, and the interface at the front of barrel (coordinate greater than 3.5m) reaches the maximum temperature in the non-interior ballistic period.

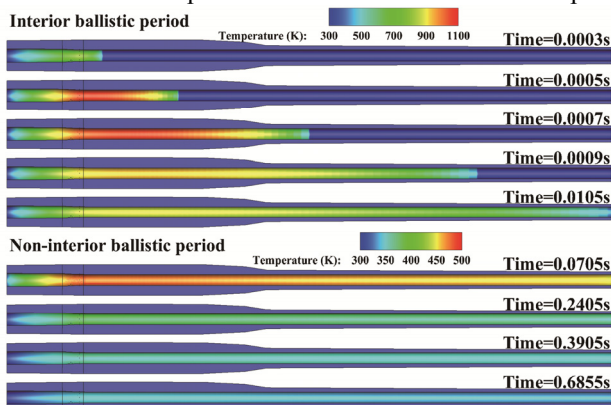


Fig. 11. Temperature distribution on the plane of fluid-solid interface

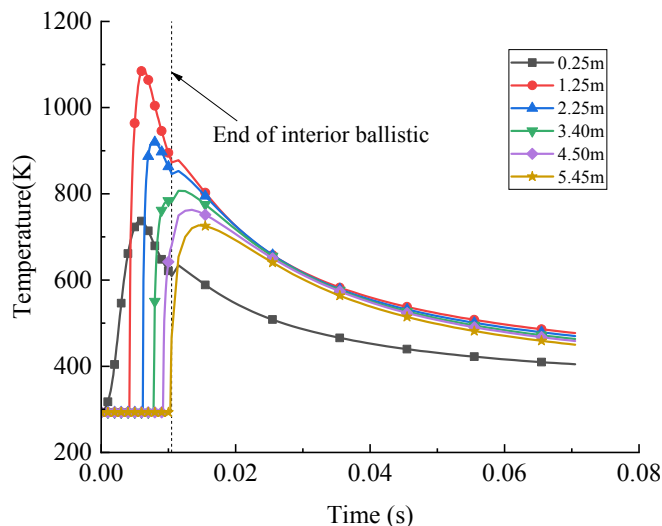


Fig. 12. Temperature curve of the monitoring point at the fluid-solid interface

(3) Solid domain temperature

The inner wall of the solid domain absorbs heat from the internal fluid by convection heat transfer, and the outer wall of the solid domain releases heat to the air and external water through convection heat transfer, and heat conducts in the calculation domain. The above factors affect the temperature distribution of the solid domain. The temperature distribution of the solid domain at any time can be obtained by numerical analysis. Six cross sections corresponding to different

coordinates were selected along the central axis as monitoring surfaces. The monitoring surfaces with coordinate values of 1.25m, 2.25m, 3.4m, and 4.5m are covered by water jacket. The monitoring surface with coordinate values of 0.25m (close to the breech) and the monitoring surface with coordinates of 5.45m (close to the muzzle) are not covered by water jacket.

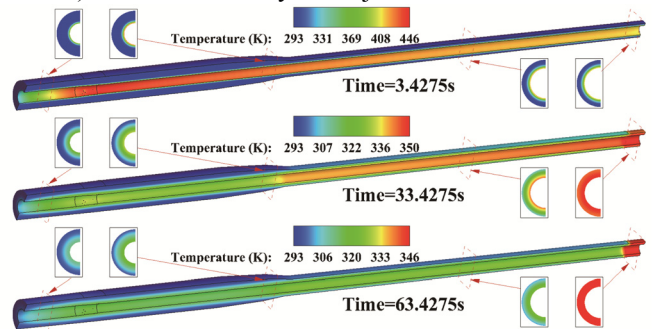
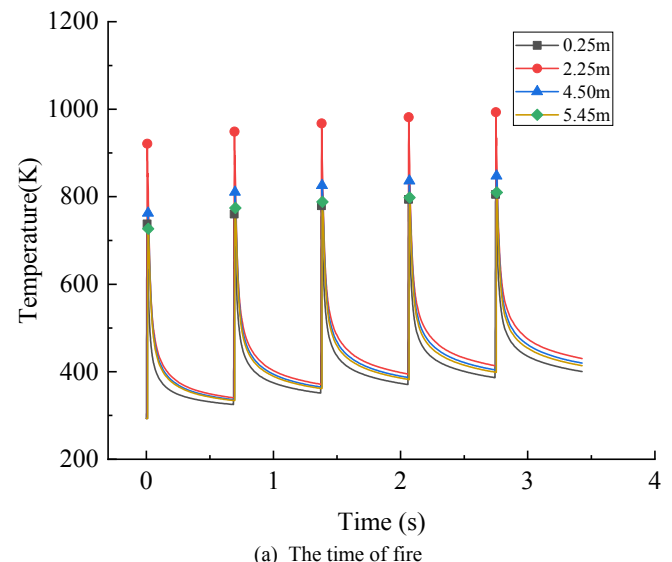


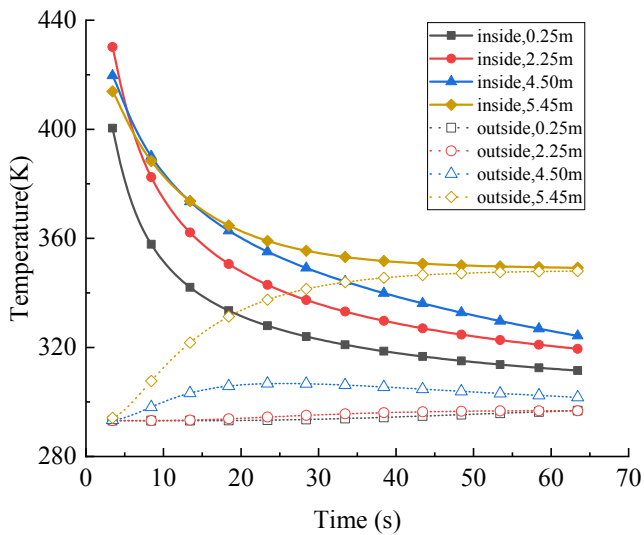
Fig. 13. Temperature distribution of the solid domain in simulation

In order to analyze the temperature distribution law of the barrel along the axial direction, firstly, the temperature distribution changes of the solid domain were calculated in the course of 5 consecutive firings and cooling for 1 minute. (This calculation process is called Simulation 1)

Figure 13 shows the temperature distribution of the barrel at three moments in Simulation 1. The images are displayed in 3D view, which are the end of 5 consecutive firings, the 30 seconds of ceasefire, and the 1 minutes of ceasefire. The contours show that during the firing process, the temperature near the chamber throat is the highest and the temperature on both sides is relatively low, which is determined by the Lagrange hypothesis of post-ballistic space. The temperature distribution of the cross-section shows that the heat is initially concentrated on the inner wall surface and gradually conducted to the outside surface, showing a gradient distribution. After stopping firing, the spray cooling system stops working, only the external water cooling system keeps working. The muzzle gradually becomes the region with the highest temperature, and the inner and outer wall surfaces form an obvious temperature boundary line. This is because the muzzle part is not wrapped by the external cooling system, and the convection heat transfer between the barrel and the external is slow.



(a) The time of fire



(b) The time of ceasefire

Fig. 14. Temperature curve of the solid domain in simulation 1

The temperature curve of the inner wall surface during the firing stage (Fig. 14.a) shows that the overall temperature of the inner wall surface is gradually rising during the 5 consecutive firings. The temperature near the chamber throat (coordinate 2.25m) is the highest and the temperature on both sides is lower. Figure 14.b shows the temperature curves of the inner and outer wall surfaces after the ceasefire. The temperature of the inner wall surface gradually decreases, and its temperature curve is not only related to the thickness of the barrel wall, but also to whether the cooling water jacket is covered. Because the time span of Simulation 1 is too short, there is no obvious temperature change on the outer wall surface of the thicker position (0.25m and 2.25m) of the barrel. The thinnest part of the barrel wall, that is, the temperature of the outer wall surface (5.45m) near the muzzle rises rapidly, and tends to be equal to the inner wall surface. However, the barrel wall at coordinates 2.25m is thin and covered by water jacket, and the temperature of the outer wall surface increases first and then decreases.

In order to compare the temperature distribution of the barrel with and without the cooling system, the temperature of the solid domain in the course of 24 consecutive firings and cooling for 5 minute in both cases was calculated simultaneously. (This calculation process is called Simulation 2)

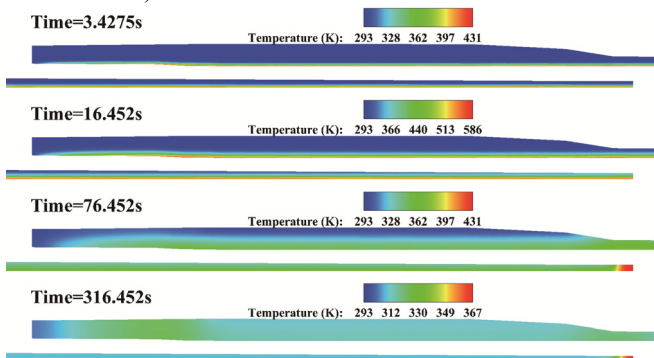


Fig. 15. Temperature distribution of the solid domain in simulation 2. (With cooling system)

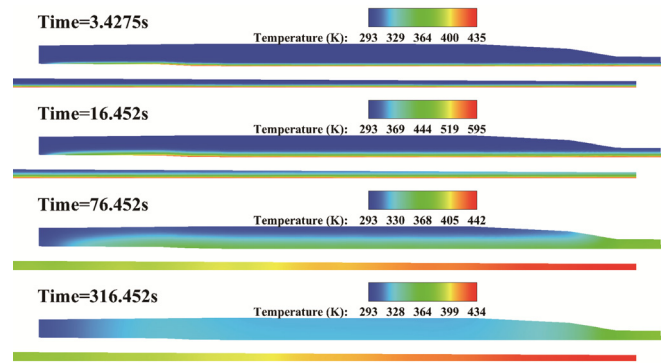
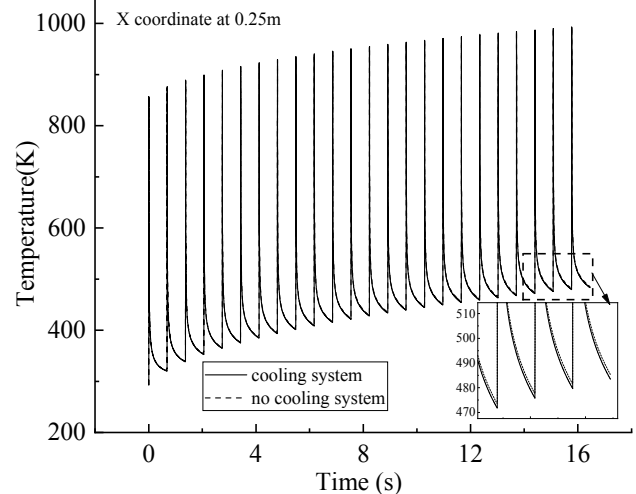
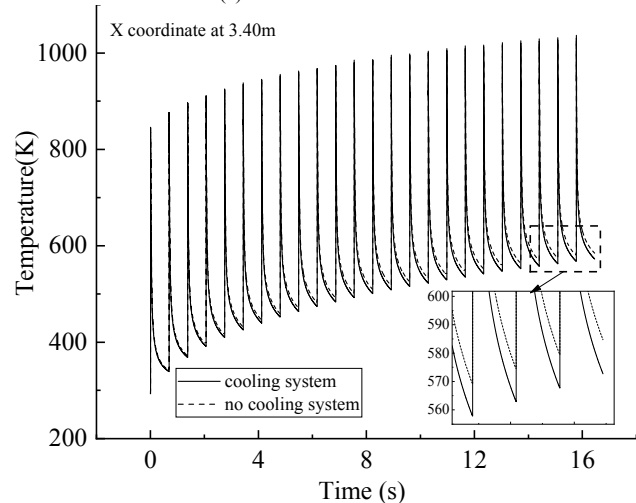


Fig. 16. Temperature distribution of the solid domain in simulation 2. (Without cooling system)

Figure 15 and Figure 16 show the temperature distribution of the barrel at four moments in Simulation 2, which are the end of 5 consecutive firings, the end of 24 consecutive firings, the 1 minutes of ceasefire, and the 5 minutes of ceasefire. The images were displayed in 2D axisymmetric view. Due to the large length-diameter ratio of the body tube, the image was divided into two sections for display. The contours show that the cooling system reduces the maximum temperature in the barrel. After 5 minutes of cooling, the temperature distribution in the radial direction of the barrel became uniform, but the temperature distribution in the axial direction was still uneven. The external circulating water cooling system can significantly reduce the temperature of the barrel area covered by the water jacket, whereas the temperature of the uncovered muzzle end and the breech end is higher.



(a) X coordinate at 0.25m



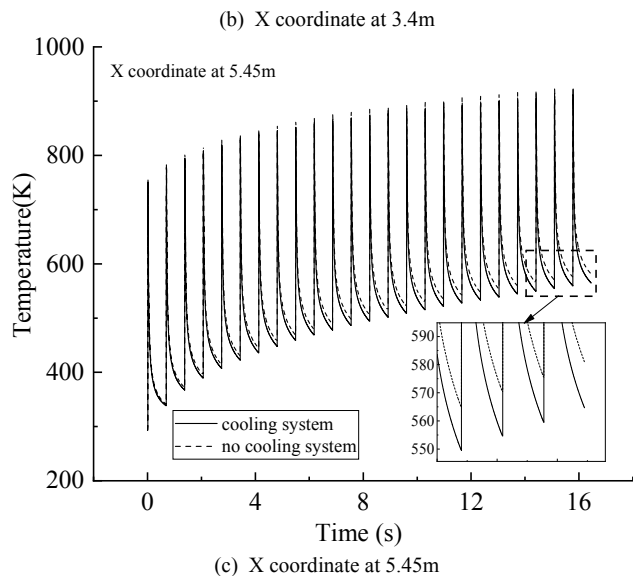


Fig.17. Temperature curve of the solid domain in simulation 2. (Inner wall surface and firing time)

The temperature curve of the inner wall surface during the firing stage in Simulation 2 is shown in Figure 17, and the influence of the cooling system at three coordinate points was compared. At this stage, most of the heat in the barrel has not been transmitted to the outer wall surface, and the external cooling system has no effect on the temperature curve of the inner wall surface, so the difference in the curve is determined by the internal cooling system. Figure 17.b and Figure 17.c show that the internal cooling system can reduce the temperature of the inner wall surface from the chamber throat to the muzzle, and the cooling effect is more obvious as it is closer to the muzzle. However, there is almost no cooling effect near the breech of barrel shown in Figure 17.a. This is because the internal cooling inlet is near the chamber throat. The distribution of water, vapor and nitrogen in Fig.4, Fig.5, and Fig.6 shows that the internal cooling does not affect the section from breech to nozzle. After 24 consecutive firings, the internal cooling system reduced the temperature of the inner wall surface of the middle section of the barrel (coordinate 3.4m) by about 12K, and reduced the temperature of the inner wall surface near the muzzle (coordinate 5.45m) by about 17K. The internal spray system has a certain cooling effect, but it is not obvious. This is because the barrel absorbs most of the heat before the internal cooling system works.

The temperature curve of the inner wall surface during the ceasefire and cooling stage in Simulation 2 is shown in Figure 18, and only the external circulating water cooling system works at this stage. As the cooling time increases, the inner wall surface temperature gradually decreases. The temperature curves with coordinate values of 0.25m and 1.25m are almost independent of external cooling factors. This is because the rear part of the autofrettaged gun barrel is thicker, and the external cooling system cannot affect the temperature of inner wall surface for a short time. The curves with coordinate values of 2.25m, 3.4m, and 4.5m show that the cooling system significantly reduces the temperature, and the larger the coordinate value, the better the cooling effect, which is related to the wall thickness of the barrel at different positions. The curve with the coordinate value of 5.45m

shows that the temperature is reduced slightly. Although the muzzle position is not covered by the water jacket, the wall of the barrel is thin and close to the water jacket. The axial heat conduction causes heat to be lost.

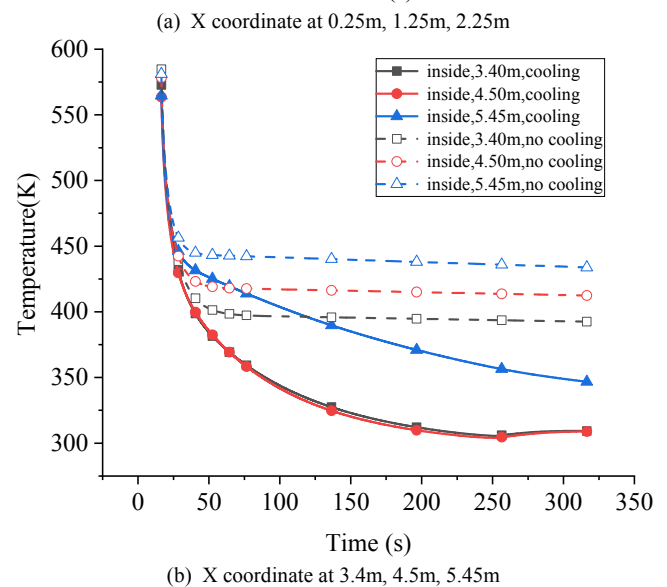
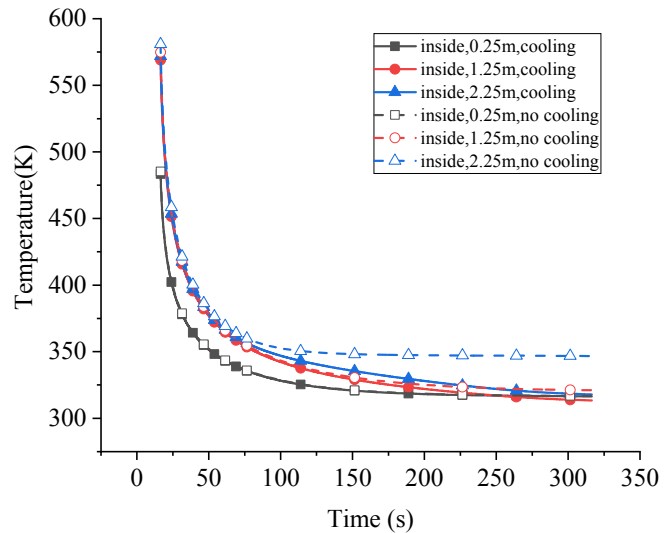


Fig.18. Temperature curve of the solid domain in simulation 2. (Inner wall surface and cease firing time)

The temperature curve of the outer wall surface during the ceasefire and cooling stage is shown in Figure 19. The two curves at coordinates 0.25m approximately coincide, indicating that the cooling system has little effect on the temperature of the outer wall surface near the breech which is not covered by the water jacket. The curves at coordinates 1.25m, 2.25m, 3.4m, 4.5m show that the temperature of the outer wall surface covered by the external cooling system is greatly reduced. The temperature curve at coordinate 5.45m has been reduced to a certain extent, indicating that the outer wall surface of the muzzle area not covered by the water jacket is also affected by the external cooling system. The temperature curves of the four locations covered by the external cooling system show that the outer wall surface temperature rises rapidly first, then gradually decreases due to the influence of cooling water, and finally the temperature rises again slightly. The reason for the rise is because the hot water flowing out of the water jacket re-enters the cooling system through circulation. This indicates that the volume

and heat dissipation of the water storage tank will also affect the cooling performance of the external cooling system.

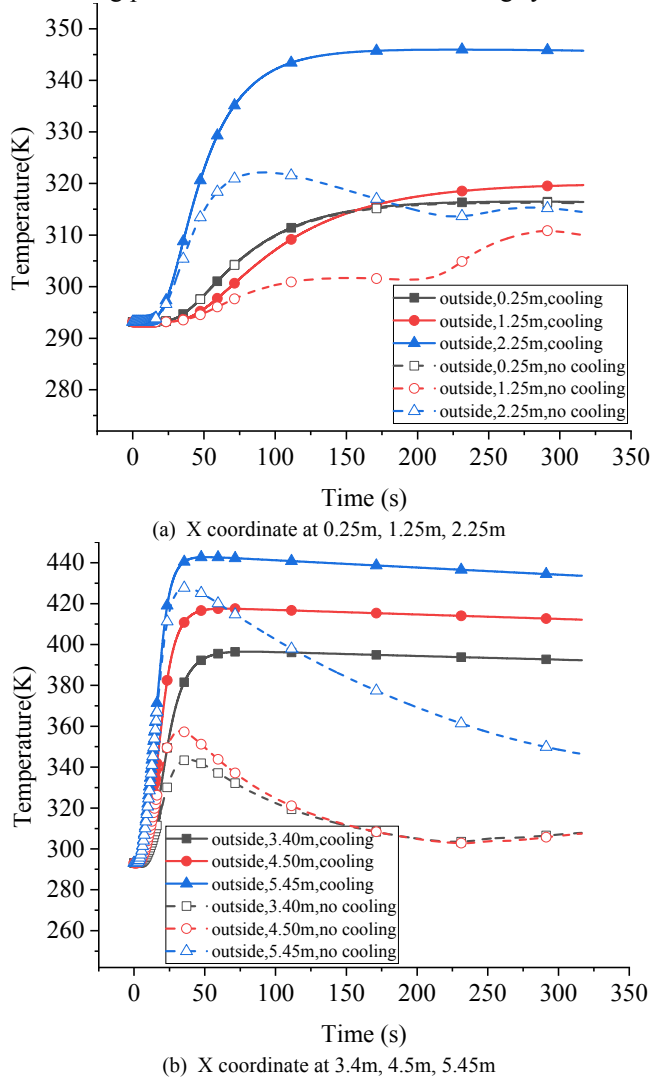


Fig.19. Temperature curve of the solid domain in simulation 2. (Outer wall surface and all time)

V. CONCLUSIONS

(1) A numerical analysis method based on CFD was proposed in this paper. This method can more accurately solve the physical quantities of the 100mm naval gun barrel when it involves both internal spray cooling and external circulating water cooling.

(2) The internal space of the barrel is extremely complex, involving high-speed and high-temperature fluid, phase transition, interphase interaction, species diffusion, etc. Compared with the traditional method of simplifying the internal fluid domain with the classical interior ballistics theory, the model can more intuitively obtain the changes and laws of various physical quantities in the fluid domain. For example, the flow trend and streamline shape of water, the shape and motion state of vapor and nitrogen groups, the irregular distribution of mixed fluid velocity, and the process of high temperature fluid being pushed out of the muzzle by the cooling system. This provides theoretical support for the internal cooling system, and provides a method reference for the efficiency optimization and structural improvement of the internal cooling system.

(3) The temperature variation of the naval gun barrel during continuous firing, ceasefire and cooling was accurately calculated, and the axial and radial temperature distribution rules were obtained. Compared with the case without cooling system, the "double cooling" system can significantly reduce the overall temperature of the barrel. The internal spray cooling system can effectively reduce the temperature peaks and valleys of the inner wall surface during continuous firing, and the closer to the muzzle, the more the temperature decreases, but the overall cooling effect is limited. The external circulating water cooling system can significantly reduce the temperature in the area covered by the water jacket. However, as the cooling time goes on, the overall temperature of the circulating water in the water storage tank rises, and the cooling efficiency gradually decreases.

(4) Although the model can analyze and predict the results to some extent, there are still some limitations. There are many simplifications and assumptions in classical interior ballistics, which have a great influence on the accuracy of the temperature, velocity, and pressure of the fluid in the model. In the following studies, we will try to replace the classical interior ballistics with the combustion theory of solid propellant particles to further improve the accuracy of numerical analysis based on multiphase flow.

REFERENCES

- [1] Б. Б. Орloff, Э. К. Ларман, Б. Г. Маликов, Construction and design of barrel, National Defence Industry Press (1982).
- [2] Z.Q. Ma, Feasibility analysis of modification of H/PJ87 single 100mm naval gun, CFHI Technology 73 (1997) pp.37-41.
- [3] W.Q. Gu, Analysis of French Mark2 100mm compact naval gun, CFHI Technology 73 (1997) pp.42-45.
- [4] L.M. Chen, Study on thermal property of composite barrel, Nanjing University of Science & Technology (2005).
- [5] Ercan Deg'irmenci, Celal Evci, Thermo-mechanical analysis of double base propellant combustion in a barrel, Applied Thermal Engineering 102 (2016) pp.1287-1299.
- [6] W. Wang, Analysis of the heat transfer in a naval gun barrel and evaluating it's erosion, North University Of China (2015).
- [7] Y.H. Wu, Simulation of barrel temperature of a rapid-fire gun based on liquid-solid couple, Acta Armamentarii 29 (3) (2008) pp.266-270.
- [8] L.J. Zhang, Analysis and optimization of naval gun barrel cooling, Nanjing University of Science & Technology (2011).
- [9] B. Wu, G. Chen, W. Xia, Heat transfer in a 155 mm compound gun barrel with full length integral midwall cooling channels, Applied Thermal Engineering 28 (2008) pp.881-888.
- [10] B. Wu, W. Xia, Y. Tang, G. Chen, P.Q. Chen, Temperature field analysis for actively cooled barrel of large caliber gun, Acta Armamentarii 25 (3) (2004) pp.267-271.
- [11] J.G. Zhao, Research on rapid-fire gun barrel cooling method, North University Of China (2013).
- [12] X.H. Wang, Thermal response analysis and active cooling system design of 155mm rapid-fire naval gun, Nanjing University of Science & Technology (2012).
- [13] T.T. Zhao, Multi-Physics coupling analysis for gun barrel, Lanzhou University of Technology (2016).
- [14] F. Moukalled, L. Mangani, M. Darwish, The finite volume method in computational fluid dynamics, Springer International Publishing Switzerland (2016).
- [15] E. Gawronska, R. Dyja, N. Sczygiol, Simulations of solidification in the presence of liquid phase movement, Proceedings of The World Congress on Engineering and Computer Science (2019) pp.342-348.
- [16] A. I. Kurbanaliev, A. R. Maksutov, G. S. Obodoeva, B. R. Oichueva, Using OpenFOAM multiphase solver interFoam for large scale modeling, Proceedings of The World Congress on Engineering and Computer Science (2019) pp.366-370.
- [17] J. Yang, P.H. Teng, H.W. Zhang, Experiments and CFD modeling of high-velocity two-phase flows in a large chute aerator facility,

- Engineering Applications of Computational Fluid Mechanics 13 (1) (2019) pp.48-66.
- [18] C. Yuan, J.C. Song, M.H. Liu, Comparison of compressible and incompressible numerical methods in simulation of a cavitating jet through a poppet valve, *Engineering Applications of Computational Fluid Mechanics* 13 (1) (2019) pp.67-90.
- [19] W.S. Tao, *Numerical heat transfer*, Xi'an Jiaotong University Press (2017).
- [20] A. Rincón-Casado, F.J. Sánchez de la Flor, 3D internal forced convection heat-transfer correlations from CFD for building performance simulation, *Engineering Applications of Computational Fluid Mechanics* 12 (1) (2018) pp.553-566.
- [21] B.J. Qian, Y.W. Wu, J.F. Chang, Y.M. Ding, *Concise heat transfer manual*, Higher Education Press (1985).
- [22] Z.M. Jin, *Interior ballistics of gun*, Beijing Institute of Technology Press (2004).
- [23] O. Redlich and J. N. S. Kwong, On the Thermodynamics of Solutions. An Equation of State. Fugacities of Gaseous Solutions, *Chem. Rev.* 44. 3. (2008) pp. 529-545.
- [24] W.H. Lee, A Pressure Iteration Scheme for Two-Phase Modeling, Technical Report LA-UR 79-975. Los Alamos Scientific Laboratory, Los Alamos, New Mexico. (1979).
- [25] *Fluent User's Guide*, ANSYS Documentation (2019).